Article:
Pei, Y, Paton, DA and Knipe, RJ (2014) Defining a 3-dimensional trishear parameter space to understand the temporal evolution of fault propagation folds. Journal of Structural Geology, 66. 284 - 297. ISSN 0191-8141

https://doi.org/10.1016/j.jsg.2014.05.018

List of Figures and Tables

Figure 1. Fault-bend fold and fault-propagation fold based on kink bend method (a, b) (Suppe, 1983; Suppe and Medwedeff, 1990) and a natural example showing variable layer thickness (c) (Allmendinger, 1998).

Figure 2. Conceptual model of trishear algorithm, based on Hardy and Ford (1997).

Figure 3. Three-dimensional parameter space with corresponding trishear models. The three axes represent the trishear p/s ratio, the trishear apical angle and the reverse fault dip, respectively.

Figure 4. Clusters of natural trishear examples in the three-dimensional parameter space. In the parameter space, 13 natural examples are plotted in and two clusters are observed. The clusters suggest that the most applicable trishear p/s ratio is 2-3 and the trishear apical angle varies from 30° to 100°. The majority of these natural trishear examples show shallow fault dips of 25°-45°.

Figure 5. Diagram delineating the impact of the selection of the reference level, i.e., the horizon used to calculate the deformation stage $\boldsymbol{Ri}$. Here a trishear model (left) with the parameters p/s ratio of 2.5, fault dip of 30° and apical angle of 50° is selected, in which we only calculate the $\boldsymbol{Ri}$ of the horizons that have not been propagated through by the underlying fault. The deformation stage $\boldsymbol{Ri}$ is not unique for a trishear model, but is variable for different horizons. The right diagram suggests a decreasing $\boldsymbol{Ri}$ value from h8 to h1 upward through the model.

Figure 6. Parameter space of trishear models with suggested parameters from the clusters of natural trishear examples.

Figure 7. Quantification of strain (ratio of hanging wall uplift versus folded bed width) associated with trishear algorithm. The figure (a) delineates the trigonometric relationship among the variables, while the apical angle versus p/s ratio plot is

generated with known strain $\boldsymbol{e}$ = 0.5, deformation stage $\boldsymbol{Ri}$ = 1 and fault dip $\boldsymbol{\alpha}$ = 45° in (b).

Figure 8. (a1-3): Trishear forward models of an upward-shallowing reverse fault. The fault dip changes from 20° to 70° upwards with a stepwise increment of 10°. (b1-3): Trishear forward models of an upward-shallowing reverse fault. The fault dip changes from 70° to 20° upwards with a stepwise decrement of 10°.

Figure 9. Trishear forward models of reverse faults affected by pre-existing faults. (a & b) upward-steepening reverse faults developed above deeper pre-existing reverse faults. (c & d) upward-shallowing reverse fault developed above deeper pre-existing reverse faults. Pre-existing faults with the same or opposite thrusting directions are all simulated.

Figure 10. The workflow of applying trishear algorithm to the Lenghu5 structure, Qaidam Basin, Northern Tibetan Plateau.

Figure 11. The forward trishear models depicts the structural evolution of the Lenghu5 structure by allowing multiple curved reverse faults in trishear forward modelling.

Table 1. A cluster of natural trishear examples in published studies and their corresponding best-fit parameters.

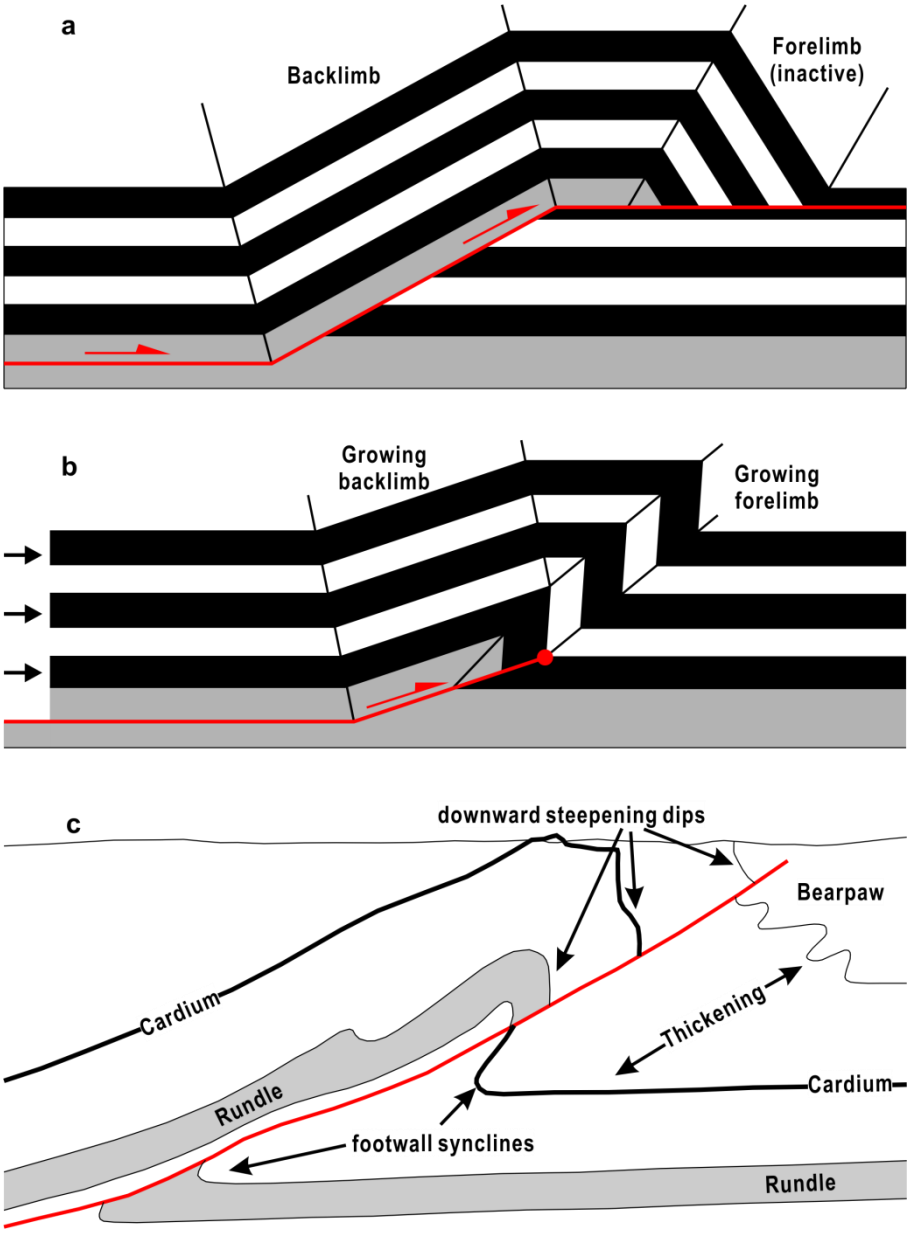

Figure 1. Fault-bend fold and fault-propagation fold based on kink bend method (a, b) (Suppe, 1983; Suppe and Medwedeff, 1990) and a natural example showing variable layer thickness (c) (Allmendinger, 1998).

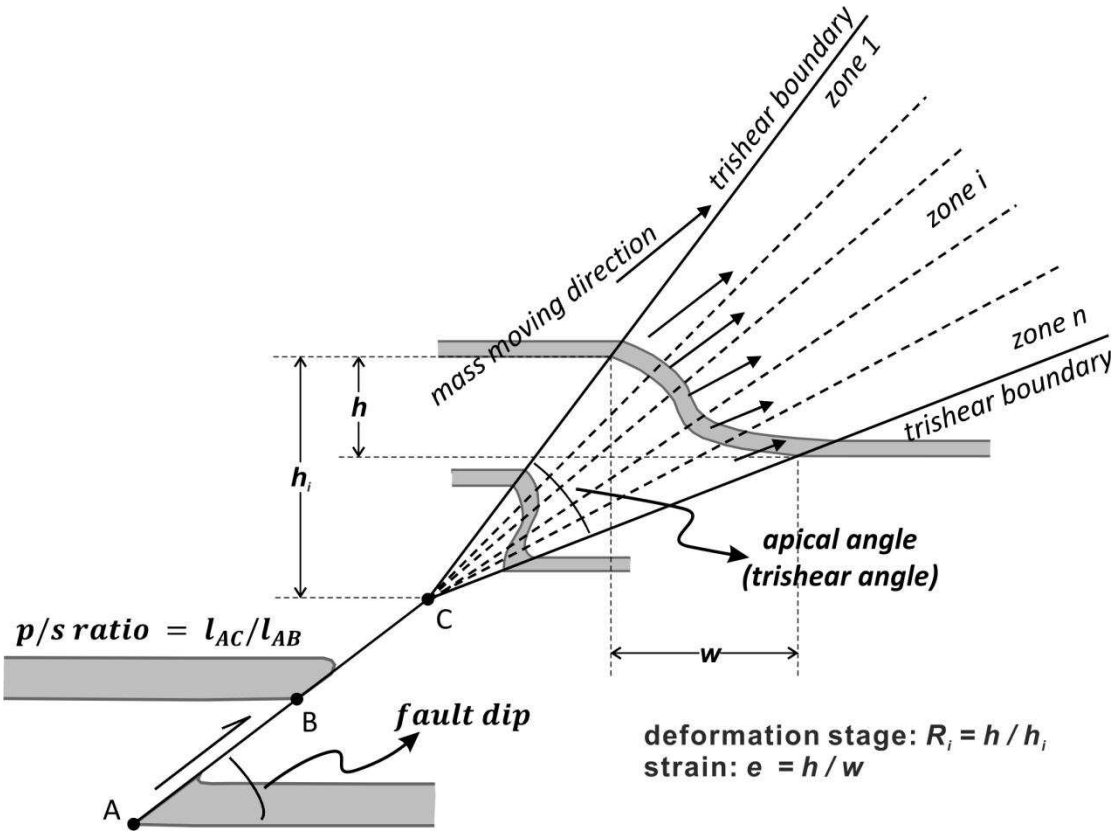

Figure 2. Conceptual model of trishear algorithm, based on Hardy and Ford (1997).

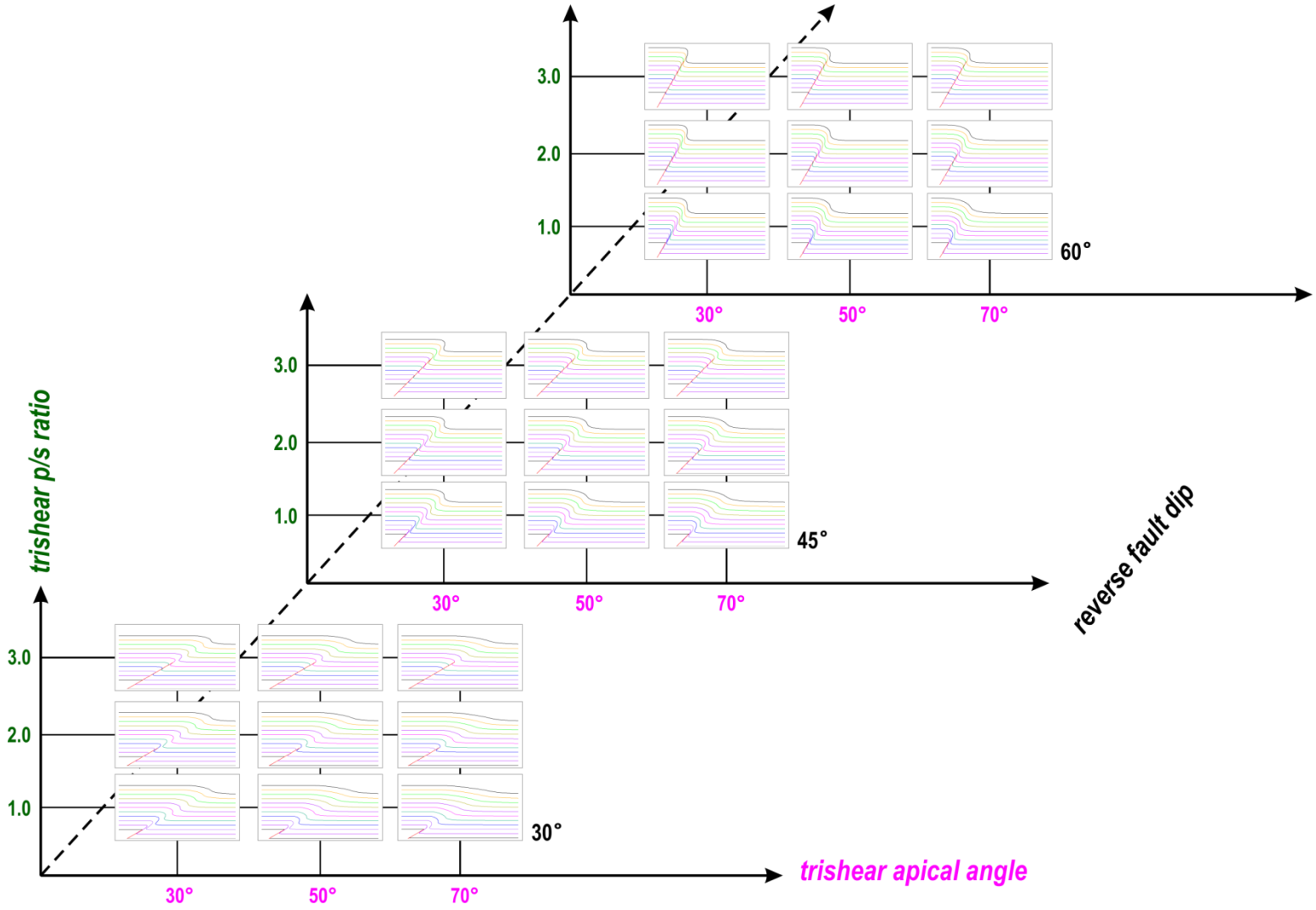

Figure 3. Three-dimensional parameter space with corresponding trishear models. The three axes represent the trishear p/s ratio, the trishear apical angle and the reverse fault dip, respectively.

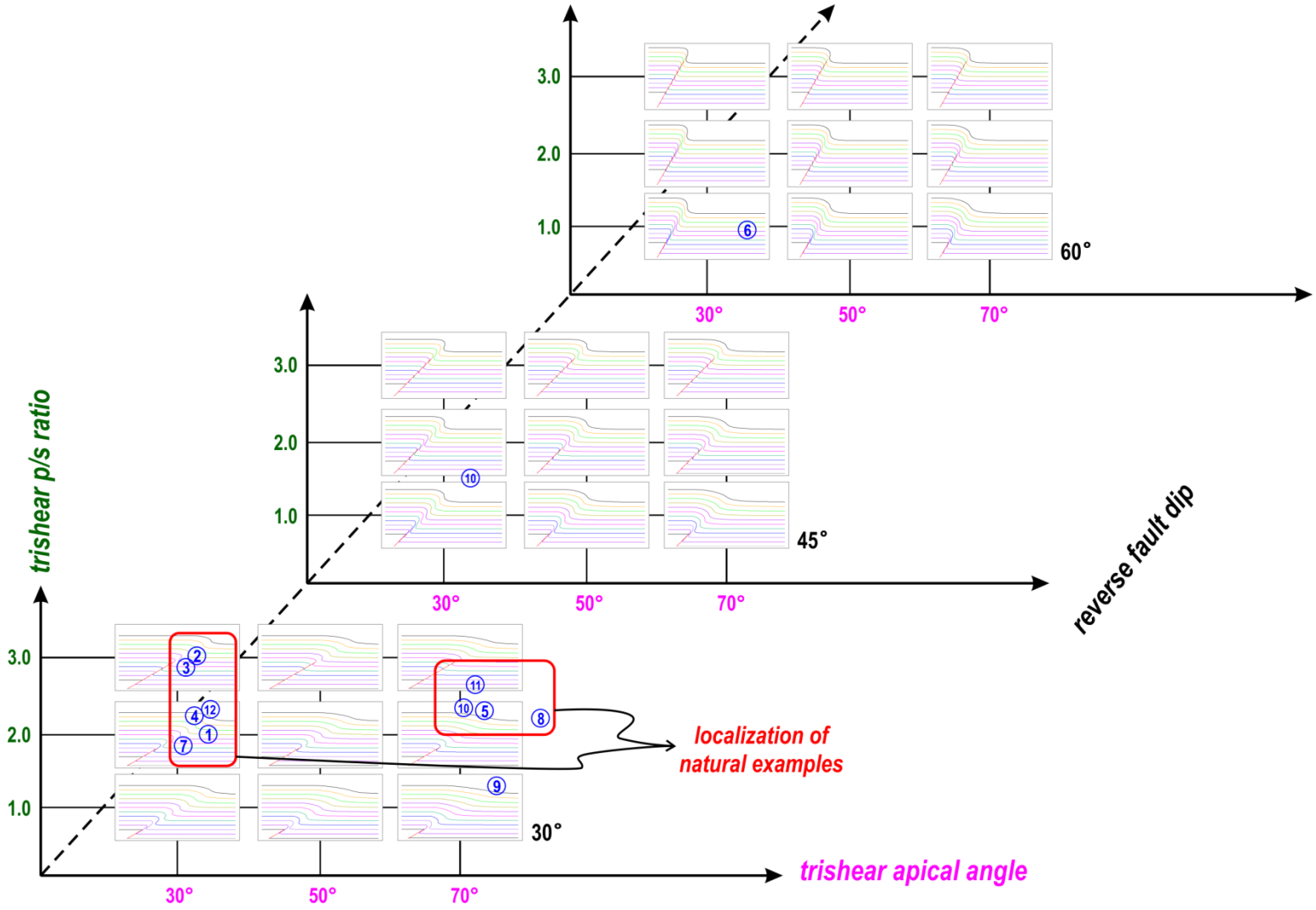

Figure 4. Clusters of natural trishear examples in the three-dimensional parameter space. In the parameter space, 13 natural examples are plotted in and two clusters are observed. The clusters suggest that the most applicable trishear p/s ratio is 2-3 and the trishear apical angle varies from 30° to 100°. The majority of these natural trishear examples show shallow fault dips of 25°-45°.

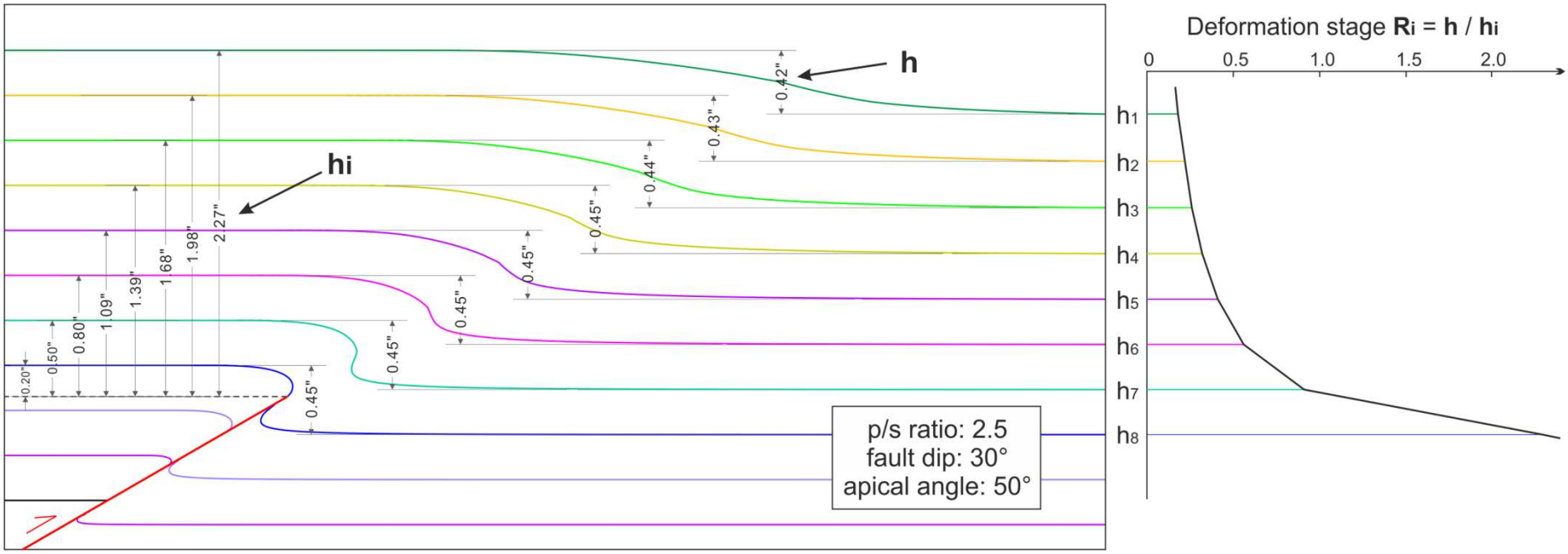

Figure 5. Diagram delineating the impact of the selection of the reference level, i.e., the horizon used to calculate the deformation stage $\boldsymbol{R_i}$. Here a trishear model (left) with the parameters p/s ratio of 2.5, fault dip of 30° and apical angle of 50° is selected, in which we only calculate the $\boldsymbol{R_i}$ of the horizons that have not been propagated through by the underlying fault. The deformation stage $\boldsymbol{R_i}$ is not unique for a trishear model, but is variable for different horizons. The right diagram suggests a decreasing $\boldsymbol{R_i}$ value from h8 to h1 upward through the model.

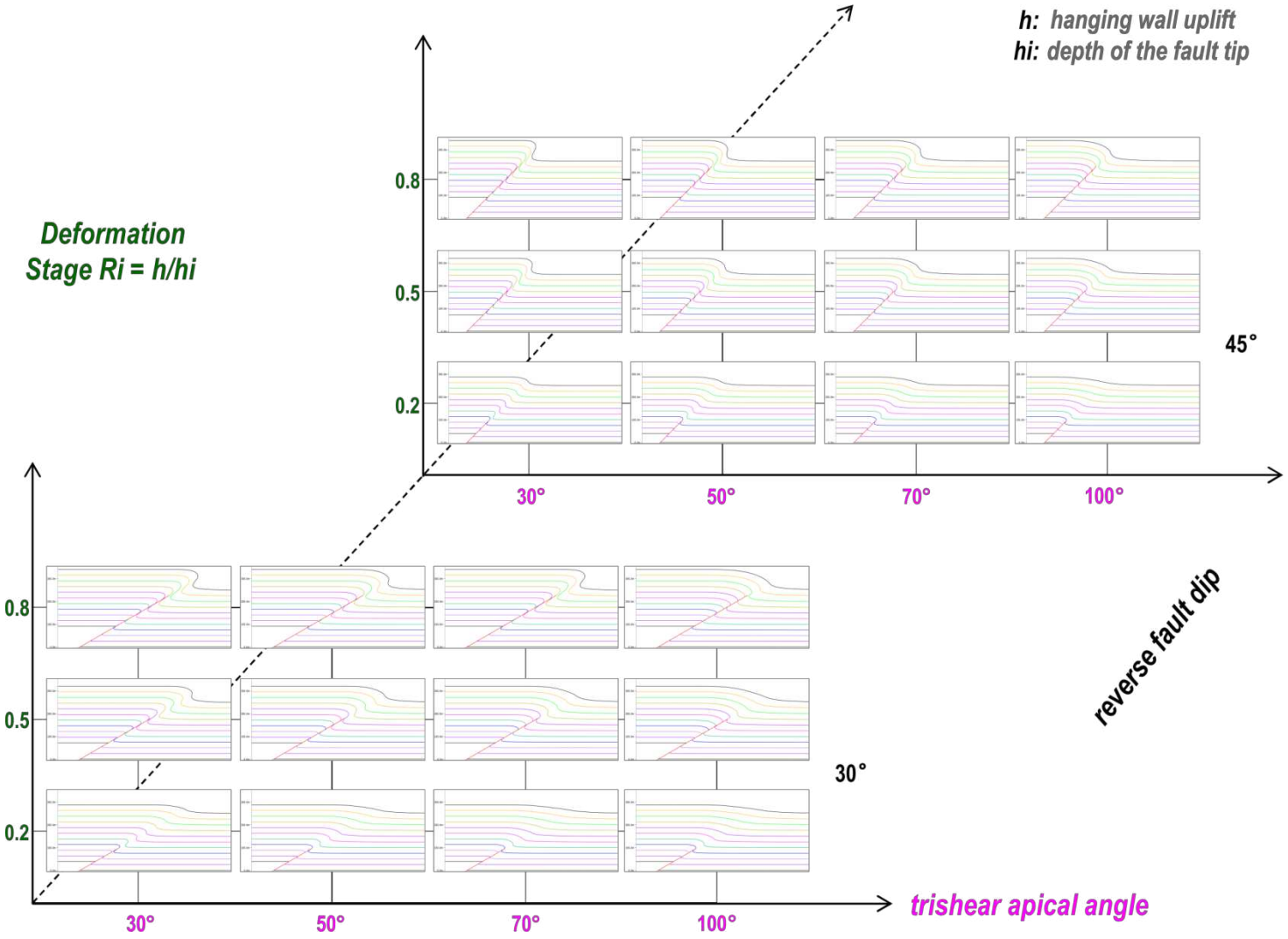

Figure 6. Parameter space of trishear models with suggested parameters from the clusters of natural trishear examples.

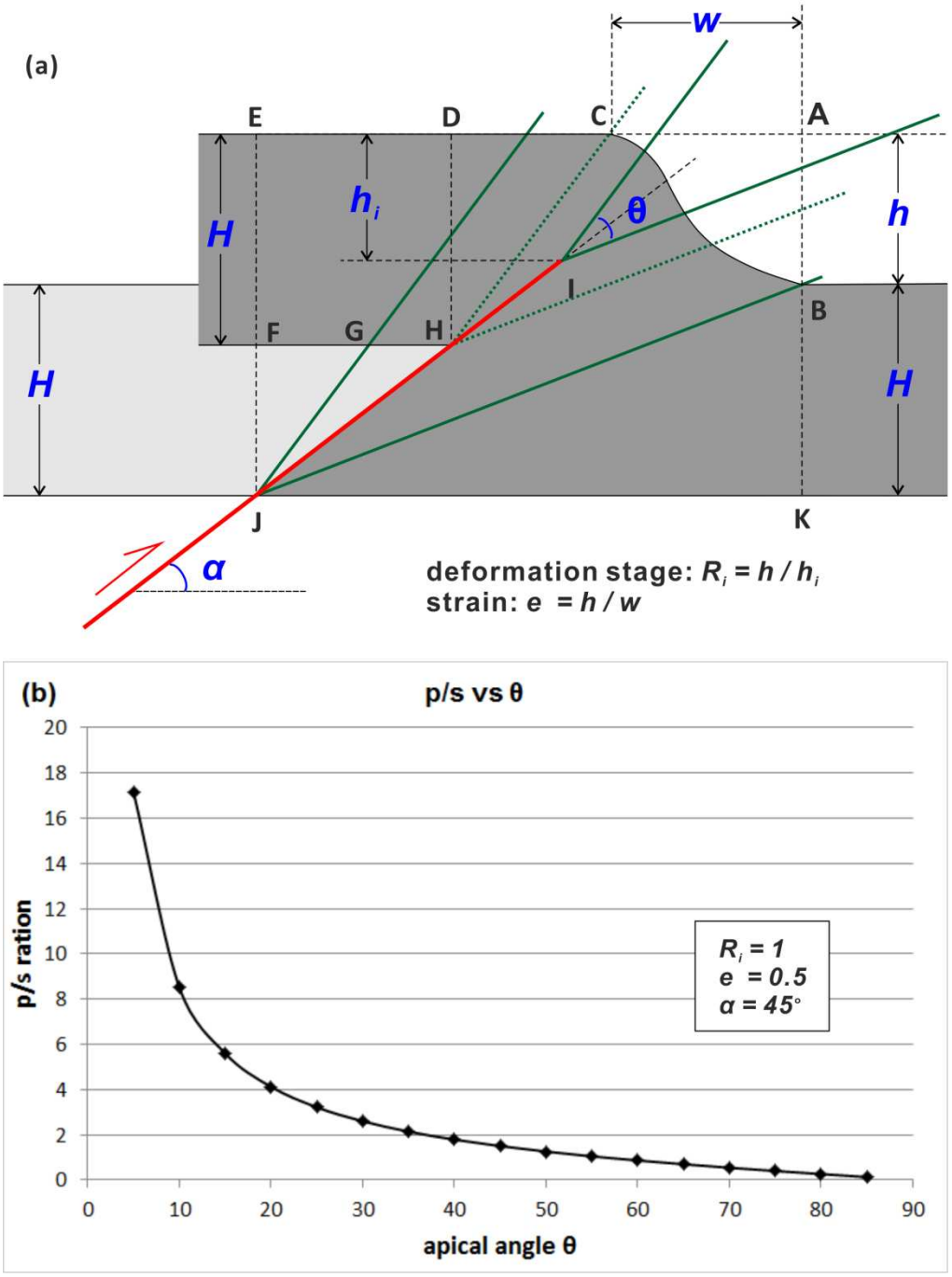

Figure 7. Quantification of strain (ratio of hanging wall uplift versus folded bed width) associated with trishear algorithm. The figure (a) delineates the trigonometric relationship among the variables, while the apical angle versus p/s ratio plot is generated with known strain $\boldsymbol{e}$ = 0.5, deformation stage $\boldsymbol{R_i}$ = 1 and fault dip $\boldsymbol{\alpha}$ = 45° in (b).

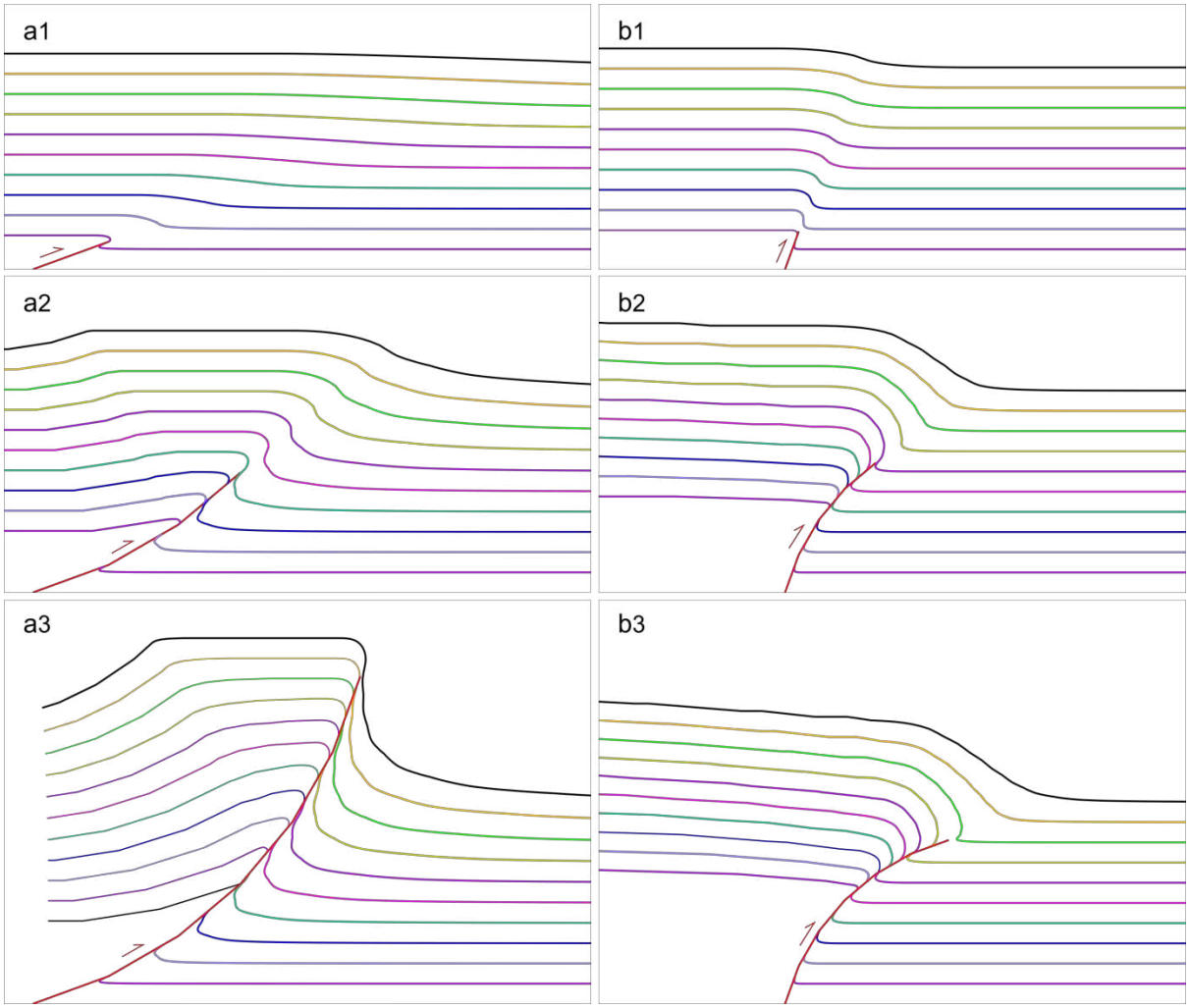

Figure 8. (a1-3): Trishear forward models of an upward-shallowing reverse fault. The fault dip changes from 20° to 70° upwards with a stepwise increment of 10°. (b1-3): Trishear forward models of an upward-shallowing reverse fault. The fault dip changes from 70° to 20° upwards with a stepwise decrement of 10°.

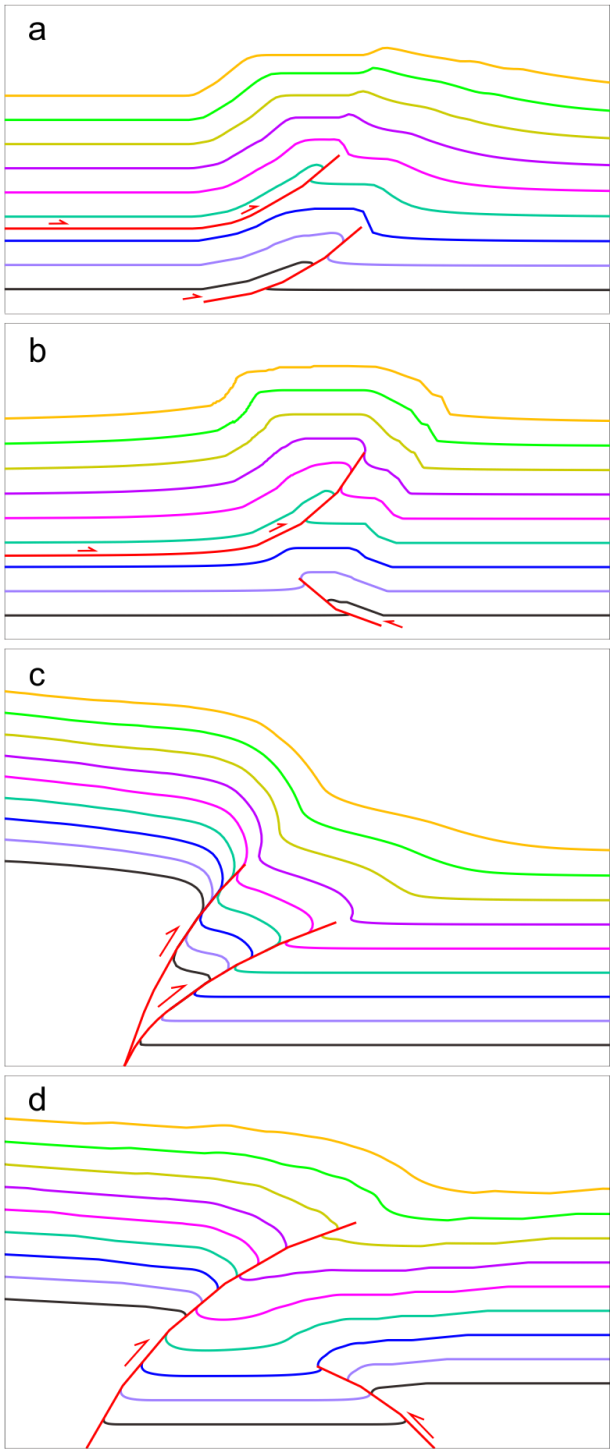

Figure 9. Trishear forward models of reverse faults affected by pre-existing faults. (a & b) upward-steepening reverse faults developed above deeper pre-existing reverse faults. (c & d) upward-shallowing reverse fault developed above deeper pre-existing reverse faults. Pre-existing faults with the same or opposite thrusting directions are all simulated.

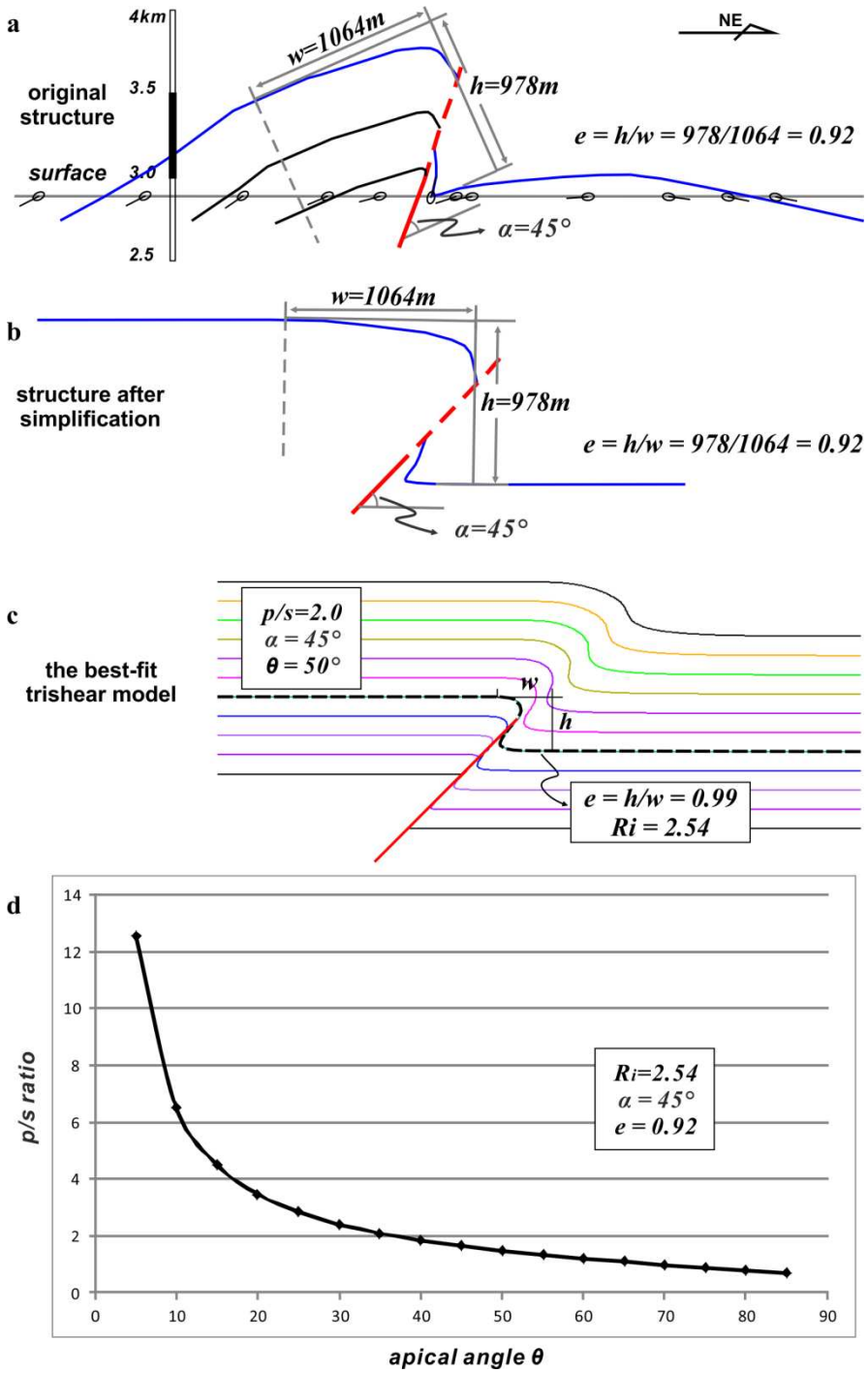

Figure 10. The workflow of applying trishear algorithm to the Lenghu5 structure, Qaidam Basin, Northern Tibetan Plateau.

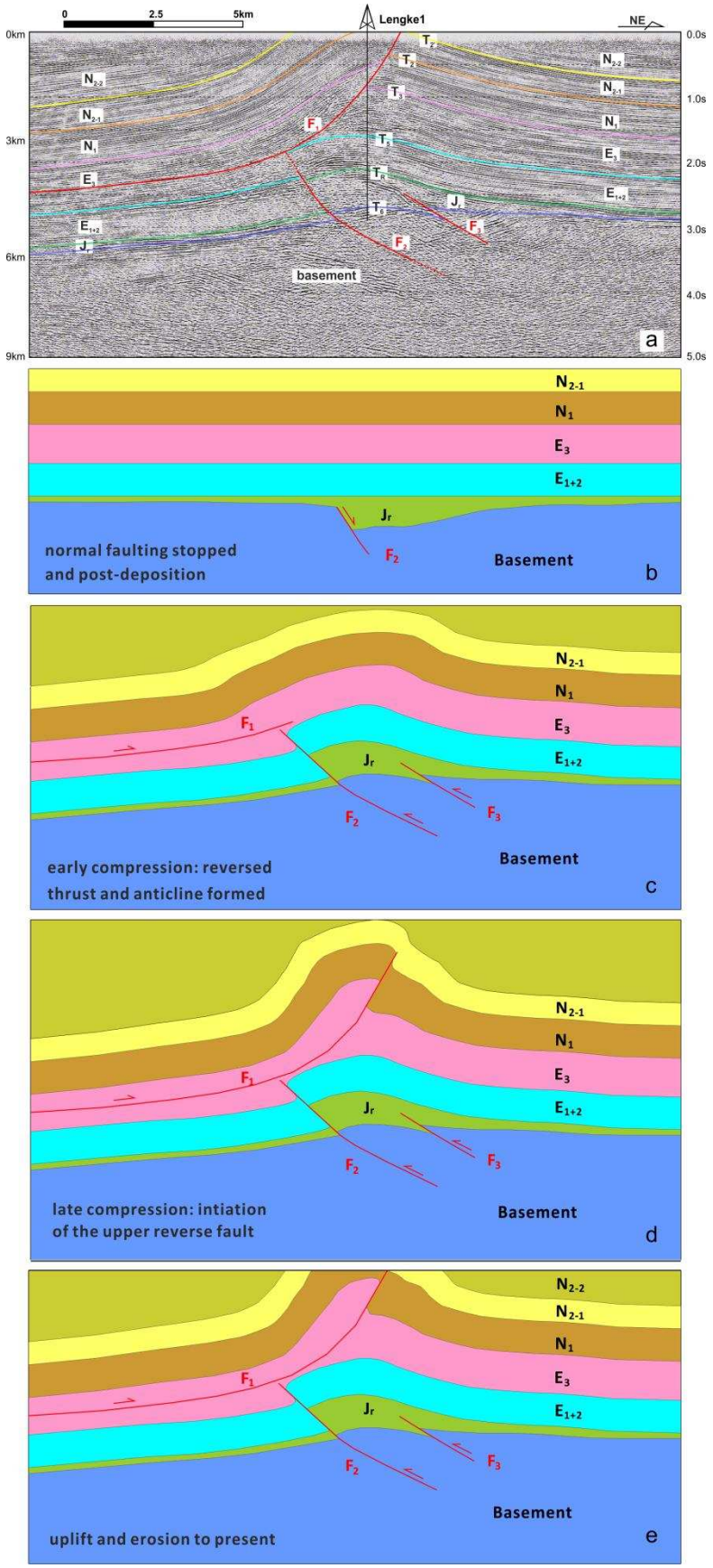

Figure 11. The forward trishear models depicts the structural evolution of the Leng-hu5 structure by allowing multiple curved reverse faults in trishear forward modelling.

Tables

Table 1. A cluster of natural trishear examples in published studies and their corresponding best-fit parameters.

Ref No.	Structure names	Basement-involved	p/s ratio	apical angle	fault dip	Scale, fault slip or stratigraphy	Example Sources
1	Turner Valley, Rocky Mountain	No	2.0+	37	25	Scale: 12km*30km (section width*depth); fault slip: 10km;	Hardy and Ford (1997)
2	Tejerina Fault, Spain	No	3.0+	35	30	Scale: 0.8km*1.2km; fault slip: 250m; stratigraphy: conglomerates with thin shales;	Hardy and Ford (1997)
3	Broad Haven, Pembrokeshire	No	3.0+	35	24	Scale: 6m*10m; fault slip: 2m;	Hardy and Ford (1997)
4	Hudson Valley, New York	No	2.5	30-35	36	Scale: 2km*3km; fault slip: 0.3km;	Allmendinger (1998)
5	Rangely anticline, W US	No	2.3	76	38	Scale: 6km*12km; fault slip: 4.2km;	Allmendinger (1998)
6	Reelfoot Fault, Proctor, US	Yes	0.9	36	80	Scale: 0.5km*0.8km; fault slip: 52m;	Champion et al. (2001)
7	Filo Morado structure, W Neuquen basin	No	1.9	35	30-40	Scale: 4km*10km; fault slip: 8.7km; stratigraphy: thick units (evaporates & shales)	Allmendinger et al. (2004)
8	Waterpocket anticline, S Utah	No	2.25	105	35	Scale: 5km*10km; fault slip:3.8km;	Cardozo (2005)
9	Rip Van Winkle anticline, New York	No	1.5	90	25	Scale: 5km*8km; fault slip:43m; stratigraphy: wackstone, packstone and grainstone;	Cardozo et al. (2005)
10	Dalong fault, Gansu, China	Yes	1.5	30	50	Scale: 5km*10km; fault slip:669m; stratigraphy: basement + cover (terrestrial clastic sediments);	Gold et al. (2006)
11	Chelungpu fault, Taiwan	No	2.5	80	35	Scale: 5m*40m; fault slip: 6m; stratigraphy: clay, silt clay with sand;	Lin et al. (2007)
12	Hudson Valley, New York	No	2.4	36	35	Scale: 2km*3km; fault slip: 0.3km;	Cardozo and Aanonsen (2009)
13	Santa Fe Springs anticline, Los Angeles basin	No	2.52	71	29	Scale: 7km*12km; fault slip:6.7km;	Cardozo and Aanonsen (2009)